表4 切除不能の非小細胞肺がんに対する放射線化学療法の第II相無作為化試験

No. Pts	Induction CT	RT(66Gy)＋CT	CR (%)	RR (%)	MST (m)	3年生存率 (%)
62	Gem 1,250mg/m² Day 1, 8, 22, 29 CDDP 80mg/m² Day 1, 22	Gem 600mg/m² Day43, 50, 64, 71 CDDP 80mg/m² Day43, 64	13	74	18.3	28
58	PTX 225mg/m² Day 1, 22 CDDP 80mg/m² Day 1, 22	PTX 135mg/m² Day43, 64 CDDP 80mg/m² Day43, 64	33	67	14.8	19
55	VNR 25mg/m² Day 1, 8, 15, 22, 29 CDDP 80mg/m² Day 1, 22	VNR 15mg/m² Day43, 50, 64, 71 CDDP 80mg/m² Day43, 64	29	73	17.7	23

Gem：gemcitabine, CDDP：cisplatin, PTX：paclitaxel, VNR：vinorelbine, RT：radiotherapy, CR：complete response, RR：response rate, MST：median survival time （文献[18]より引用）

に検討した報告では，AHFRTとSTDRTでは生存に差を認めなかった[1]．したがって，局所進行非小細胞肺がんに対して，1回1.2Gyもしくは1.5Gyの1日2回分割照射を行っても治療成績を改善することは難しいと考えられる．

近年ではcontinuous hyperfractionated accelerated radiotherapy(CHART)やhyperfractionated accelerated radiation therapy(HART)など1日3回照射の成績が報告されている[15)~17)]．CHARTとは週末も含め12日間連続で1日3回，1.5Gy，計54Gyの照射を行う方法である[15)]．STDRTとCHARTを比較した第III相試験ではCHARTで有意に生存期間が延長していたものの，この結果は放射線治療単独による第III相試験であった．化学放射線併用療法の無作為化試験でCHARTが使われた報告はない．HARTは週末を除く週5日にわたり，1日3回，4時間ごと(脊髄照射野では8時間ごと)に合計57.6Gyを照射する照射方法である[16)17)]．カルボプラチン＋パクリタキセルによる導入化学療法後に行ったHARTとSTDRTとを比較した第III相試験の結果がEastern Cooperative Oncology Group(ECOG)より報告されている[16)]．この臨床試験は患者登録が不良であったために早期に中止となったが，HART群の治療成績は比較的良好で，生存期間中央値はSTDRT群14.9か月に対してHART群20.3か月であり，毒性は許容範囲であった[16)]．Ishikuraらはシスプラチン＋ビノレルビンに続くHARTのpilot studyの結果を報告している[17)]．この試験には30名が登録され，全体として奏効率は83％で，生存期間中央値は24か月であり，2年，3年生存率もそれぞれ50％と32％であった[17)]．化学療法とCHARTもしくはHARTを組み合わせた臨床試験の今後の展開が注目される．

抗がん剤の選択

シスプラチン＋ビンデシン，シスプラチン＋エトポシドなどの前世代の化学療法の組み合わせでは，放射線同時併用を行う際に化学療法単独での投与量を全量投与することが可能であったが，1990年代に開発された第3世代抗がん剤では放射線治療と併用した場合，毒性が増強するために減量が必要である[18)~20)]．放射線治療と化学療法を同時併用する場合に，どの併用化学療法が一番効果的であるかに関しては十分な臨床試験の成績が得られていない．Cancer and Leukemia Group B(CALGB)は切除不能の局所進行非小細胞肺がんに対し，シスプラチンに，第3世代抗がん剤であるゲムシタビン，パクリタキセル，ビノレルビンを2剤併用した2コースの導入化学療法の後に，放射線治療を晩期同時併用する無作為化第II相試験を行った(表4)[18)]．しかしながら，シスプラチンは導入化学療法期も放射線併用期も同量を使用することが可能で

あったが，ゲムシタビン，パクリタキセル，ビノレルビンは放射線併用に際しては約半量に減量せざるをえず，そのためか生存期間も中央値で14～17か月と従来の化学放射線同時併用療法の成績を凌駕するものではなかった．

カルボプラチン＋パクリタキセルを週1回放射線治療と併用する方法が米国では比較的汎用されていたが，CALGBが報告した第Ⅲ相試験の結果では生存期間は従来の化学療法と放射線治療よりも劣る結果であった[21]．したがって，現在までのところ週1回もしくは連日低用量の化学療法を放射線治療と併用する方法の有用性は示されていない．

分子標的治療薬

Epidermal growth factor receptor (EGFR) チロシンキナーゼ阻害剤であるgefitinib, erlotinib, cetuximabは非小細胞肺がんの分子標的治療薬としてもっとも期待できる薬剤である[22]．*In vitro* の研究では，EGFR阻害剤は放射線治療を組み合わせることで相乗効果が期待できるとされている[23][24]．CALGB30106とオーストラリアで実施された第Ⅰ相試験ではⅢ期非小細胞肺がんの放射線化学療法にgefitinibを加えても毒性が増強することはなかった[25]．また，シカゴ大学の第Ⅰ相試験ではⅢ期の非小細胞肺がんに対する化学放射線療法とerlotinib併用の評価が行われた[26]．このようにgefitinibまたはerlotinibと化学放射線治療との組み合わせによって局所進行非小細胞肺がんの治療成績を向上させる試みがなされている．JCOGでは局所進行非小細胞肺がんに対するシスプラチンとビノレルビンによる導入化学治療に続きgefitinibと放射線治療を同時併用する治療の安全性と効果を検討する臨床試験を開始している (JCOG0402-MF)．この試験の目的は，安全性および有効性を確認することであり，primary endpointは安全性 (Grade 2以上の肺臓炎を認めずにプロトコール治療を完遂できた割合)，secondary endpointsは，1年生存率，奏効率，全生存期間，無増悪生存期間，有害事象発生割合，重篤な有害事象発生割合である．「Grade 2以上の肺臓炎を認めずにプロトコール治療を完遂できた症例の割合」の期待値を75%とし，閾値を55%，$\alpha=0.1, \beta=0.1$として症例数を設定すると37例が必要となり，治療を開始した37例中25例以上がGrade 2以上の肺臓炎を認めずに治療を完遂した場合に，本治療は実施可能と判断される．

Southwest Oncology Group (SWOG) は2005年米国臨床腫瘍学会総会 (ASCO：American Society of Clinical Oncology) で切除不能Ⅲ期非小細胞肺がんに対してシスプラチン＋エトポシド＋根治的放射線治療後に引き続きドセタキセルによる地固め療法を施行後gefitinibまたはプラセボによる維持療法の有用性を検討する第Ⅲ相試験 (SWOG0023) の中間解析結果を発表した[27]．この試験では，試験を継続しても当初期待された効果が証明できる可能性がないことが判明し試験が中止された．この理由は不明であり，EGFR変異，FISHおよびK-rasに関する分子レベルでの解析を含めた調査を現在実施している．

さらに最近では血管新生阻害薬と放射線治療との組み合わせが注目されている．血管新生阻害薬であるangiostatinと放射線治療を併用した基礎実験では，毒性を増悪させることなく腫瘍消退に成功したという報告がある[28]．抗VEGF抗体であるbevacizumabを抗がん剤と併用することにより大腸がん，乳がんなどで生存が延長することが最近の第Ⅲ相試験で示され，扁平上皮がんを除くⅣ期非小細胞肺がんでも延命効果が示されている．したがって，局所進行非小細胞肺がんの治療成績向上の方法として化学放射線治療とbevacizumabの併用療法が期待されている．また，thalidomideは血管新生阻害剤としてよく知られている薬であるが，ECOGはⅢ期非小細胞肺がんの治療としてカルボプラチン＋パクリタキセルと放射線治療にthalidomideを加える群，加えない群とを比較した第Ⅲ相試験を展開している (ECOG3598)[29]．肺がんに過剰発現するcyclooxygenase-2 (COX-2) は予後不良因子であり，COX-2阻害薬は化学療法と放射線治療の効果を高める可能性が示唆されている．ただし，選択性COX-2阻害薬使用による心血管系に対する安全性の懸念があるため注意が必要である[30]．

おわりに

限局型小細胞肺がんでは，シスプラチン＋エ

トポシドによる併用化学療法にAHFRTによる放射線治療を早期に同時併用し，CRとなった症例には予防的全脳照射を追加することが標準治療として確立されている．しかし，局所進行非小細胞肺がんに対する標準的治療法はいまだ確定していない．シスプラチンを使った化学療法と胸部放射線治療の同時併用は，切除不能の局所進行非小細胞肺がんの5年生存率を約15%にまで改善したが，その成績は満足できるものではない[1)3)9)]．分子標的治療薬gefitinib, erlotinib, cetuximab, bevacizumabなどの導入は，局所進行非小細胞肺がんの治療成績をさらに向上させるものとして期待されており，切除不能局所進行非小細胞肺がんに対するより良い標準的治療を確立するために，積極的に臨床試験を実施する必要がある．

文　献

1) Ohe Y, Ishizuka N, Tamura T, et al. Long-term follow-up of patients with unresectable locally advanced non-small cell lung cancer treated with chemoradiotherapy : a retrospective analysis of the data from the Japan Clinical Oncology Group trials (JCOG 0003A). Cancer Sci 2003 ; 94 : 729.
2) Van Meerbeek JP, Kramer G, Van Schil PE, et al. A randomized trial of radical surgery (S) versus thoracic radiotherapy (TRT) in patients (pts) with stage IIIA-N2 non-small cell lung cancer (NSCLC) after response to induction chemotherapy (ICT) (EORTC 08941). Proc Am Soc Clin Oncol 2005 ; 23 : 624s.
3) Furuse K, Fukuoka M, Kawahara M, et al. phase III study of concurrent versus sequential thoracic radiotherapy in combination with mitomycin, vindesine, and cisplatin in unresectable stage III non-small cell lung cancer. J Clin Oncol 1999 ; 17 : 2692.
4) Nagai K, Tsuchiya R, Mori T, et al. A randomized trial comparing induction chemotherapy followed by surgery with surgery alone for patients with stage IIIA N2 non-small cell lung cancer (JCOG 9209). J Thorac Cardiovasc Surg 2003 ; 125 : 254.
5) Ohe Y, Yamamoto S, Suzuki K, et al. Risk factors of treatment-related death in chemotherapy and thoracic radiotherapy for lung cancer. Eur J Cancer 2001 ; 37 : 54.
6) Ohe Y. Treatment-related death from chemotherapy and thoracic radiotherapy for advanced cancer. Panminerva Med 2002 ; 42 : 205.
7) Non-small Cell Lung Cancer Collaborative Group. Chemotherapy in non-small cell lung cancer : a meta-analysis using updated data on individual patients from 52 randomised clinical trials. BMJ 1995 ; 311 : 899.
8) Sculier JP, Paesmans M, Lafitte JJ, et al. A randomized phase III trial comparing consolidation treatment with further chemotherapy to chest irradiation in patients with initially unresectable locoregional non-small-cell lung cancer reaponding to induction chemotherapy. Ann Oncol 1999 ; 10 : 295.
9) Curran WJ, Scott CB, Langer CL, et al. Long-term benefit is observed in a phase III comparison of sequential vs concurrent chemo-radiation for patients with unresected stage III nsclc : RTOG 9410. Proc Am Soc Clin Oncol 2003 ; 22 : 621.
10) Kubota K, Watanabe K, Kunitoh H, et al. Phase III randomized trial of docetaxel plus cisplatin versus vindesine plus cisplatin in patients with stage IV non-small-cell lung cancer : the Japanese Taxotere Lung Cancer Study Group. J Clin Oncol 2004 ; 22 : 254.
11) Fournel P, Robinet G, Thomas P, et al. Randomized phase III trial of sequential chemoradiotherapy compared with concurrent chemoradiotherapy in locally advanced non-small-cell lung cancer : Groupe Lyon-Saint-Etienne d'Oncologie Thoracique-Groupe Français de Pneumo-Cancerologie NPC 95-01 Study. J Clin Oncol 2005 ; 23 : 5910.
12) Zatloukal PV, Petruzelka L, Zemanova M, et al. Concurrent versus sequential chemoradiotherapy with cisplatin and vinorelbine in locally advanced non-small cell lung cancer : a randomized study. Lung Cancer 2004 ; 46 : 87.
13) Sause W, Kolesar P, Taylor S, et al. Final results of phase III trial in regionally advanced unresectable non-small cell lung cancer : Radiation Therapy Oncology Group, Eastern Cooperative Oncology Group, and Southwest Oncology Group. Chest 2000 ; 117 : 358.

14) Schild SE, Stella PJ, Geyer SM, et al. Phase III trial comparing chemotherapy plus once-daily or twice-daily radiotherapy in Stage III non-small-cell lung cancer. Int J Radiat Oncol Biol Phys 2000 ; 54 : 370.
15) Saunders M, Dische S, Barrett A, et al. Continuous hyperfractionated accelerated radiotherapy (CHART) versus conventional radiotherapy in non-small-cell lung cancer : a randomised multicentre trial. CHART Steering Committee. Lancet 1997 ; 350 : 161.
16) Belani CP, Wang W, Johnson DH, et al. Phase III study of the Eastern Cooperative Oncology Group (ECOG 2597) : induction chemotherapy followed by either standard thoracic radiotherapy or hyperfractionated accelerated radiotherapy for patients with unresectable stage III A and B non-small-cell lung cancer. J Clin Oncol 2005 ; 23 : 3760.
17) Ishikura S, Ohe Y, Nihei K, et al. A phase II study of hyperfractionated accelerated radiotherapy (HART) after induction cisplatin (CDDP) and vinorelbine (VNR) for stage III non-small-cell lung cancer (NSCLC). Int J Radiat Oncol Biol Phys 2005 ; 61 : 1117.
18) Vokes EE, Herndon JE, Crawford J, et al. Randomized phase II study of cisplatin with gemcitabine or paclitaxel or vinorelbine as induction chemotherapy followed by concomitant chemoradiotherapy for stage III B non-small-cell lung cancer : cancer and leukemia group B study 9431. J Clin Oncol 2002 ; 20 : 4191.
19) Masters GA, Haraf DJ, Hoffman PC, et al. Phase I study of vinorelbine, cisplatin, and concomitant thoracic radiation in the treatment of advanced chest malignancies. J Clin Oncol 1998 ; 16 : 2157.
20) Sekine I, Noda K, Oshita F, et al. Phase I study of cisplatin, vinorelbine, and concurrent thoracic radiotherapy for unresectable stage III non-small-cell lung cancer. Cancer Sci 2004 ; 95 : 691.
21) Vokes EE, Herndon JE, Kelley MJ, et al. Induction chemotherapy followed by concomitant chemoradiotherapy (CT/XRT) versus CT/XRT alone for regionally advanced unresectable non-small cell lung cancer (NSCLC) : Initial analysis of a randmized phase III trial. Proc Am Soc Clin Oncol 2004 ; 22 : 618s.
22) Ready N. Inhibition of the epidermal growth factor receptor in combined modality treatment for locally advanced non-small cell lung cancer. Semin Oncol 2005 ; 32 : S35.
23) Magne N, Fischel JL, Dubreuil A, et al. Sequence-dependent effects of ZD1839 ('Iressa') in combination with cytotoxic treatment in human head and neck cancer. Br J Cancer 2002 ; 86 : 819.
24) Chinnaiyan P, Huang S, Vallabhaneni G, et al. Mechanisms of enhanced radiation response following epidermal growth factor receptor signaling inhibition by erlotinib (Tarceva). Cancer Res 2005 ; 65 : 3328.
25) Ready N, Herndon J, Vokes E, et al. Initial cohort toxicity evaluation for chemoradiotherapy (CRT) and ZD1839 in stage III non-small cell lung cancer (NSCLC) : A CALGB stratified phase II trial. Proc Am Soc Clin Oncol 2004 ; 23 : 632s.
26) Mauer A, Haraf D, Hoffman PC, et al. A phase I trial of OSI774 in combination with chemoradiation (CRT) for unresectable, locally advanced non-small cell lung cancer (NSCLC). Proc Am Clin Oncol 2003 ; 22 : 651s.
27) Kelly K, Gaspar LE, Chansky K, et al. Low incidence of pneumonitis on SWOG0023 : A preliminary analysis of an ongoing phase III trial of concurrent chemoradiotherapy followed by consolidation docetaxel and Iressa/placebo maintenance in patients with inoperable stage III non-small cell lung cancer. Proc Am Soc Clin Oncol 2005 ; 23 : 634s.
28) Mauceri HJ, Hanna NN, Beckett MA, et al. Combined effects of angiostatin and ionizing radiation in antitumour therapy. Nature 1998 ; 394 : 287.
29) Merchant JJ, Kim K, Mehta MP, et al. Pilot and safety trial of carboplatin, paclitaxel, and thalidomide in advanced non-small-cell lung cancer. Clin Lung Cancer 2000 ; 2 : 48.
30) Solomon SD, McMurray JJ, Pfeffer MA, et al. Cardiovascular risk associated with celecoxib in a clinical trial for colorectal adenoma prevention. N Engl J Med 2005 ; 352(11) : 1071.

Lung Cancer (2006) 52, 135–140

available at www.sciencedirect.com

SCIENCE DIRECT®

journal homepage: www.elsevier.com/locate/lungcan

Imaging of gefitinib-related interstitial lung disease: Multi-institutional analysis by the West Japan Thoracic Oncology Group

Masahiro Endo[a,*], Takeshi Johkoh[b], Kazuhiko Kimura[c], Nobuyuki Yamamoto[d]

[a] *Division of Diagnostic Radiology, Shizuoka City Hospital, Shizuoka, Japan*
[b] *Department of Medical Physics, Osaka University Graduate School of Medicine, Oasaka, Japan*
[c] *Department of Radiology, Kawasaki Hospital, Kobe, Japan*
[d] *Division of Thoracic Oncology, Shizuoka Cancer Center, Nagaizumi, Japan*

Received 10 October 2005; received in revised form 3 February 2006; accepted 6 February 2006

KEYWORDS
Gefitinib;
Interstitial lung desease;
Drug-induced lung disease;
Computed tomography;
Diffuse alveolar damage

Summary Gefitinib (Iressa™) is an epidermal growth factor receptor tyrosine kinase inhibitor that has been approved for the treatment of lung cancer in Japan, however, after marketing several cases of severe pulmonary toxicity were reported. The West Japan Thoracic Oncology Group conducted an independent survey of acute pulmonary toxicity and interstitial lung disease (ILD) caused by gefitinib in its member's institutions. The purpose of this study was to clarify the image characteristics of ILD caused by the molecular-targeting drug gefitinib. A total of 1976 patients had been treated with gefitinib between August and December 2002, and 102 of them were suspected of having acute pulmonary toxicity and ILD. A final definite diagnosis of gefitinib-induced ILD was made by at least three radiologists based on a review and analysis of the chest radiography and CT findings plus the clinical data in the medical records. The imaging findings were classified into four patterns: (A) a nonspecific area with ground-glass attenuation, (B) a multifocal area of airspace consolidations, (C) patchy distribution of ground-glass attenuation accompanied by interlobar septal thickening, and (D) extensive bilateral ground-glass attenuation or airspace consolidations with traction bronchiectasis. CT as well as chest radiography had been performed in 65 of the 102 patients at the onset of ILD, and chest radiography alone had been performed in 26. After excluding 11 cases with insufficient data and 21 cases

Abbreviations: AEP, acute eosinophilic pneumonia; AIP, acute interstitial pneumonia; BOOP, bronchiolitis obliterans organizing pneumonia; CT, computed tomography; DAD, diffuse alveolar damage; EGFR, epidermal growth factor receptor; ILD, interstitial lung disease; IPF, idiopathic pulmonary fibrosis; WJTOG, West Japan Thoracic Oncology Group

* Corresponding author. Present address: Division of Endoscopy, Shizuoka Cancer Center, Nagaizumi, Japan. Tel.: +81 55 989 5222; fax: +81 55 989 5783.
E-mail address: m.endo@scchr.jp (M. Endo).

doi:10.1016/j.lungcan.2006.02.002

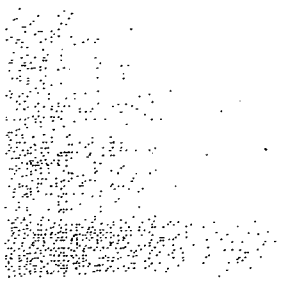

concluded to be other pulmonary diseases, 70 patients were diagnosed with gefitinib-induced ILD. Finally, the diagnostic image findings were classified as pattern A in 29 cases, pattern B in 7 cases, pattern C in 3 cases, pattern D in 20 cases and others in 11 cases. The CT images were classified as pattern A, B, C, and D in 24, 7, 1, and 12 cases, respectively. The mortality rate was significantly higher in the patients with pattern D than the other patterns. Pattern D were thought to represent the features of diffuse alveolar damage. In conclusion, the molecular-targeting drug gefitinib induces pulmonary toxicity at a certain rate and the imaging findings of ILD induced by gefitinib are similar to those of pulmonary toxicity induced by conventional antineoplastic agents.

1. Introduction

Lung cancer is the leading cause of cancer deaths among both females and males in Japan and worldwide. The epidermal growth factor receptor tyrosine kinase inhibitor gefitinib (Iressa™) was recently approved in Japan for the treatment of recurrent non-small cell lung cancer, before being approved in the United States. Clinical trials have revealed significant variability in response to gefitinib, showed higher response rate in Japanese patients than in a predominantly European-derived population (27.5% versus 10.4%, respectively in a multi-institutional phase II trial) [1]. The good responders in Japan were women, patients with adenocarcinoma, and non-smokers. Adverse drug reactions in the pre-approved trials were frequent, but mild, and included an acne-like skin rash and diarrhea. However, some cases of gefitinib-related life-threatening interstitial lung disease (ILD) have been reported since the marketing of the drug [2–6], and the incidence of ILD was considered higher than that of ILD caused by pre-existing anticancer drugs. Based on these considerations, the West Japan Thoracic Oncology Group (WJTOG) independently investigated the incidence of acute pulmonary toxicity and ILD, the risk factors for their development, and the outcome. The radiological diagnosis of acute pulmonary toxicity and ILD in that survey was made by the participating radiologists. The purpose of this study was to clarify the characteristics of pulmonary toxicity induced by the molecular-targeting drug gefitinib based on an analysis of diagnostic images alone.

2. Materials and methods

We observed the guidelines for the retrospective epidemiological analysis in Japan using encoded data of patients in order to survey the incidence and risk factors of gefitinib-related ILD, and the survey by the WJTOG was approved by the review board of each institution.

2.1. Patients

The chest computed tomography (CT) scans and chest radiographs obtained in the 102 patients with suspected gefitinib-related ILD were retrospectively reviewed. The patients were identified as follows.

We requested to examine the number of patients who had begun to receive gefitinib between August 31, 2002 (when the drug was put on the National Health Insurance Drug List) and December 31, 2002, and the number of patients who were suspected of acute pulmonary toxicity and ILD to the 112 centers that were members of the WJTOG at the end of December 2002, and responses were obtained from 84 centers. A total of 1976 patients had been treated with gefitinib, and 102 of them were suspected of having acute pulmonary toxicity and ILD. In addition, a thorough clinical history and record of the patients and their chest radiography and CT scans taken about 1 month before the onset of ILD, at the onset, and serially after the onset, were obtained from each institution. Chest radiography and CT scans taken about 1 month before the onset were obtained for 97 and 92 patients, respectively, and chest radiography and CT scans taken at the onset were obtained for 92 and 65 patients, respectively. Serial chest radiography and CT scans after the onset were obtained for 89 and 32 patients, respectively. The patients consisted of 15 females and 87 males, and their mean age was 67 years (range, 38–90 years). All patients had non-small cell lung cancer including adenocarcinoma in 69 patients, squamous cell carcinoma in 27 patients, large cell carcinoma in 2 patients, and others in 4 patients. No patients had undergone lung biopsy and/or bronchoalveolar lavage to diagnose ILD.

2.2. Radiography and CT scanning methods

The chest radiographs obtained were the original films taken at each institution and included conventional films and computed radiographs. The CT scans were performed with a CT unit at each institution. All CT scans were obtained with 5–10 mm collimation at 5–10 mm intervals and with the patient in the supine position and at maximal inspiration. In 40 cases thin-section CT was performed with 1–2 mm collimation at 10 mm intervals at the onset of ILD. Scanning extended from the apices of lungs to the costophrenic angles. Thin-section CT images were reconstructed with a high-spatial-frequency algorithm. CT scans were obtained with window settings for lung parenchyma (window width, 1600–1800 HU; window level, −600 to −700 HU) and mediastinum (window width, 300–350 HU; window level, 25–40 HU).

2.3. Image analysis

The chest radiography and CT images were reviewed by at least three chest radiologists together, and final decisions regarding the findings were made by consensus, in conference with pulmonary physicians and medical oncologists. Gefitinib-related ILD was defined as an acute respiratory disorder that developed during gefitinib therapy in which ILD

was suspected on the basis of the imaging findings and other diseases, such as pneumonia, could be ruled out based on the clinical information.

The confirmation of the diagnosis was categorized like this: (1) proofless ILD, as defined by no chest radiography and CT at the onset of the disease, (2) non-ILD, as defined by pneumonia, progression of lung cancer, radiation pneumonitis, organizing pneumonia, and non-gefitinib related ILD, and (3) confirmed ILD, as defined by a confirmation of gefitinib-related ILD.

The CT findings were assessed for distribution and patterns of such as ground-glass attenuation, airspace consolidation, interlobular septal thickening, and traction bronchiectasis. Ground-glass attenuation was defined as an area of slightly increased attenuation in which the bronchial walls and vessels remained visible. Airspace consolidation was defined as an area of increased attenuation with obscuration of the adjacent bronchial wall and vessels, and traction bronchiectasis was defined as irregular bronchial dilatation within areas with ground-glass attenuation or airspace consolidation. Based on these findings, the CT images of gefitinib-induced ILD were classified into four patterns [7], and we defined the plain-film findings corresponding to them.

Pattern A was defined as a pattern of only nonspecific area with ground-glass attenuation, and it corresponded to diffuse and faint opacity without lung volume loss on chest radiography. Pattern B was defined as a pattern of multifocal areas of airspace consolidation such as in cryptogenic organizing pneumonia or bronchiolitis obliterans organizing pneumonia (BOOP), and it corresponded mainly to peripheral consolidations on chest radiography. Pattern C was defined as a pattern of patchy distribution of areas with ground-glass attenuation accompanied by interlobular septal thickening, such as in acute eosinophilic pneumonia (AEP), and it corresponded to patchy or diffuse faint, linear opacities on chest radiography. Pattern D was defined as a pattern of extensive bilateral ground-glass attenuation or airspace consolidations with traction bronchiectasis, such as in acute interstitial pneumonia (AIP), and it corresponded to diffuse faint opacities or consolidations with lung volume loss on chest radiography. Pre-existing lung lesions such as emphysema, IPF, old inflammation, and lung resection, etc., were also recorded.

2.4. Statistical analysis

The differences in frequency of each category in each subgroup were evaluated by the Fisher exact test or the χ^2-test with continuity correction, probability values less than 0.05 were considered significant.

3. Results

The images and data in the medical records of the 102 patients with suspected ILD were analyzed. Sixty-five patients had been examined by CT as well as chest radiography at the onset of ILD, but 26 patients had been examined by chest radiography alone. Eleven patients were considered as indeterminate for pulmonary toxicity, because no chest radiographs or CT scans at the onset were submitted, or they were insufficient. We analyzed the chest radiographs and/or CT scans of the other 91 patients in the context of the clinical course, and made a diagnosis of gefitinib-related ILD in 70 of them. The remaining 21 patients were diagnosed with other diseases; pneumonia in 9, progression of lung cancer in 4, radiation pneumonitis in 3, and other conditions in 5 (Table 1).

Table 1 Confirmation of the diagnosis of interstitial lung disease (ILD) induced by gefitinib

Category	Number of patients
Proofless ILD	11
Non-ILD	21
(1) Pneumonia (infectious disease)	9
(2) Progression of lung cancer	4
(3) Radiation pneumonitis	3
(4) Others	5
Confirmed ILD	70
Total	102

Chest radiographs of the 70 patients diagnosed with gefitinib-related ILD were classified as pattern A in 29 patients (43.8%; Fig. 1a), pattern B in 7 (10.0%; Fig. 2a), pattern C in 3 (4.3%), pattern D in 20 (28.6%; Fig. 3a), and other patterns in 11 (15.7%). The CT images were classified as pattern A, B, C, D, and other patterns in 24 patients (47.1%; Fig. 1b), 7 patients (13.7%; Fig. 2b), 1 patient (2.0%), 12 patients (23.5%; Fig. 3b), and 7 patients (13.7%), respectively. The number of deaths in each pattern was 9, 2, 0, 15, and 5, respectively, and the mortality rate was 31.0%, 28.6%, 0%, 75.0%, and 45.5%, respectively. It was significantly higher in patients with pattern D than in patients with other patterns (75.0% versus 32.0%, $p = 0.001$).

In addition, we analyzed associations between the frequency of pre-existing lung lesions and the fatal cases. There were 52 (74.1%) patients with various grades of pulmonary emphysema, 14 (20.0%) with IPF, and 20 (28.6%) with old inflammation, such as pleural thickening and/or fibrous change. Thoracic irradiation was performed in 16 (22.9%) patients, and lung resection in 17 (24.3%). No associations were found between the frequency of pre-existing lung lesions and the fatal cases (Tables 2 and 3).

Table 2 Frequency of radiological patterns of ILD induced by gefitinib and mortality

Radiological pattern	Frequency		Mortality
	Chest radiography	CT	
A	29 (43.8%)	24 (47.1%)	9 (31.0%)
B	7 (10.0%)	7 (13.7%)	2 (28.6%)
C	3 (4.3%)	1 (2.0%)	0 (0.0%)
D	20 (28.6%)	12 (23.5%)	15 (75.0%)
Others	11 (15.7%)	7 (13.7%)	5 (45.5%)
Total	70	51	31 (44.3%)

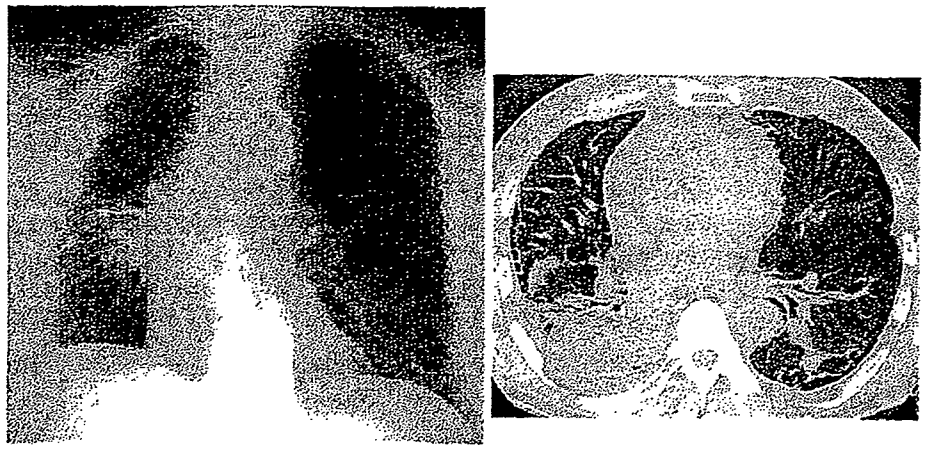

(a) (b)

Fig. 1 A 60-year-old male with stage IV non-small cell lung cancer who had been treated with platinum-based chemotherapy developed mild dyspnea on day 10 after administration of gefitinib. The chest radiography reveals a mass opacity in the right hilum and diffuse ground-glass density over the entire lung field against a background of emphysema and fibrosis (a). The CT scan shows nonspecific areas with ground-glass attenuation throughout the lung parenchyma (b).

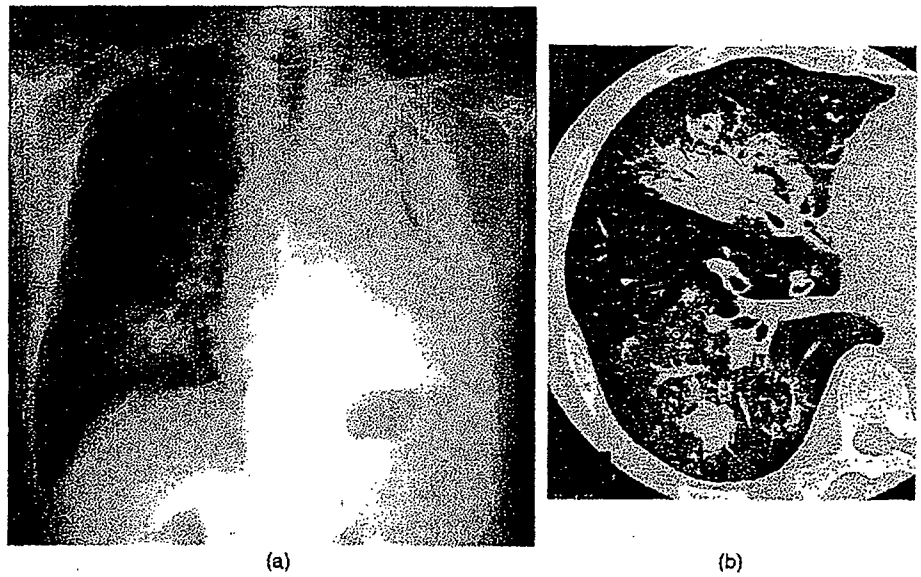

(a) (b)

Fig. 2 A 70-year-old male with stage IIIB adenocarcinoma who had been treated with platinum-based chemotherapy was started on gefitinib, and developed a severe cough and mild dyspnea on day 30 of gefitinib therapy. The chest radiography shows areas of consolidation on the upper and lower field of the right lung (a), and multifocal areas of airspace consolidation are seen on the thin-section CT scan (b).

4. Discussion

After gefitinib was approved on July 5, 2002, some cases of severe pulmonary toxicity were come to light in Japan, and AstraZeneca organized an Expert Committee analyzed about gefitinib-related ILD [8]. The WJTOG also independently conducted a survey of patients with acute pulmonary toxicity caused by gefitinib. Then we participated in a survey and had an opportunity to review the chest radiographs and CT images suspected gefitinib-related ILD.

In this study nonspecific areas with ground-glass attenuation (pattern A, 47.1%) and extensive bilateral ground-glass attenuation or airspace consolidation with traction bronchiectasis (pattern D, 23.5%) were observed on chest CT images in the majority of patients, and it was considered that the molecular-targeting drug gefitinib also showed radiological appearances of pulmonary toxicity similar to those reported to be caused by conventional antineoplastic drugs [9–13]. Those drugs are known to induce a variety of pathological reactions in the lung, such as noncardiogenic

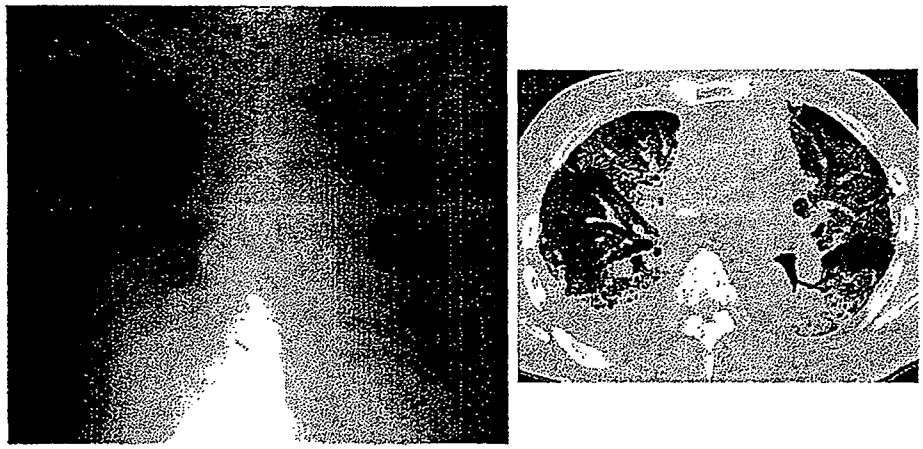

(a) (b)

Fig. 3 A 62-year-old male who had undergone right upper lobectomy complained of the acute onset of dyspnea on day 5 after the start of gefitinib therapy. The anterio-posterior chest radiography shows diffuse ground-glass densities in the lung parenchyma (a). The CT scan shows extensive bilateral ground-glass attenuation and airspace consolidations with traction bronchiectasis (b). The patient died 10 days after the onset of ILD despite treatment by steroid pulse therapy.

pulmonary edema, diffuse alveolar damage (DAD), eosinophilic pneumonia, BOOP, and chronic interstitial pneumonitis with fibrosis [9,10]. Since Akira et al. reported that the pulmonary damage by antineoplastic drugs was for the most part due to a direct cytotoxic effect and that a ground-glass attenuation was often seen on diagnostic images [10], it was assumed that the pulmonary damage caused by gefitinib was also attributable to a direct cytotoxic effect in the same way, but there is still no evidence that would make it possible to confirm that. There have been few studies on the relationship between the imaging findings and fatal cases in ILD caused by gefitinib [2,4]. In the present study the mortality rate was significantly higher in the patients with pattern D than in the patients with the other patterns. Pattern D was thought to represent the features of DAD, and this finding was consistent with the report by Ichikado et al. that traction bronchiectasis was an important prognostic CT finding in AIP [14]. On the other hand, some patients with pattern A died. However, they may have included patients whose findings should have been classified as pattern D, because the CT scanning conditions differed considerably from institution to institution and/or because breath-holding by some of the patients may have been insufficient. It is also a report claiming that ground-glass attenuation corresponds to DAD pathologically [12], and for that reason it appears that it should be borne in mind that the pattern A group may also have included cases with a poor prognosis. On the other hand, the mortality rate of pattern C was low, the same another report [12].

The AstraZeneca Expert Committee Meeting Report claims that the CT findings in ILD related by gefitinib mainly consist of patchy or diffuse ground-glass opacification and/or consolidation, and that there were no differences from the imaging findings in drug-related ILD that had been reported in the past [8]. It stated that pathological examination of the fatal cases showed that DAD was the main cause of death, and although no pathological assessment was conducted, the imaging findings in our own cases with a poor outcome suggested the same.

74.3% of the patients with gefitinib-related ILD had pre-existing pulmonary emphysema and 20% had IPF. Most of the patients had some pulmonary changes, including changes associated with surgery or radiotherapy, but the pre-existing changes were not statistically related to the imaging patterns of ILD or mortality due to ILD. Takano et al. reported that IPF was a significant risk factor for ILD according to the results of a multivariate analysis [15], but they said nothing in regard to associations with the outcome after the onset of

Table 3 Frequency of pulmonary comorbidities in surviving patients and fetal cases

Pulmonary comorbidities	Total ($n=70$)	Surviving patients ($n=39$)	Fetal cases ($n=31$)	p
Emphysema	52 (74.3%)	29 (74.4%)	23 (74.2%)	0.987
Idiopathic pulmonary fibrosis	14 (20.0%)	8 (20.5%)	6 (19.4%)	0.904
Old inflammation	20 (28.6%)	8 (20.5%)	12 (38.7%)	0.094
Thoracic irradiation	16 (22.9%)	9 (23.1%)	7 (22.6%)	0.941
Post-resection	17 (24.3%)	12 (30.8%)	5 (16.1%)	0.156
None	6 (8.6%)	3 (7.7%)	3 (9.7%)	0.768

symptoms. The AstraZeneca Expert Meeting Report, on the other hand, states that IPF is a risk factor for ILD, and at the same time that it might be a negative-prognostic factor [8]. While there seems to be no doubt that IPF is a risk factor for ILD, we would like to await a future assessment of the association with the outcome.

This study is of great significance in terms of being the first to analyze the diagnostic images of a large number of patients for pulmonary toxicity caused by a single drug, because previous studies on drug-induced pulmonary toxicity have been limited to a single center, or are an accumulation of case report [9–12]. However, this study had several limitations: (1) the CT scanning and display conditions differed from center to center, (2) thin-section CT, which is most reliable method for the diagnosis of diffuse lung disease, was performed in a small number of patients, and (3) the diagnosis of pulmonary toxicity was based on the classification of images into known patterns in the absence of pathological evidence. However, depending on the condition of patients with ILD, the diagnosis of ILD must often be made on the basis of plain chest radiography alone. Ordinary CT may add diagnostically important information, even when breath-holding is poor, and be useful in indicating the extent of the damage or whether the image pattern predicts a high probability of death. Therefore, accurate diagnosis of ILD in the early stage based on the clinical course as well as the chest radiography and/or CT findings may be important for early treatment.

In conclusion, this is the first study to demonstrate that the molecular-targeting drug gefitinib induces pulmonary toxicity at a certain rate and that the imaging findings of ILD related by gefitinib are similar to those of pulmonary toxicity related by conventional antineoplastic agents. Physicians planning to use gefitinib in the future should be thoroughly familiar with these imaging findings.

Acknowledgments

We thank the members of the West Japan Thoracic Oncology Group and its related centers for providing us with the opportunity to conduct this valuable work. This study was not supported by any specific funding source.

References

[1] Fukuoka M, Yano S, Giaccone G, et al. Multi-institutional randomized phase II trial of gefitinib for previously treated patients with advanced non-small cell lung cancer. J Clin Oncol 2003;21:2237–56.
[2] Inoue A, Saiji Y, Maemondo M, et al. Severe acute interstitial pneumonia and gefitinib. Lancet 2003;361:137–9.
[3] Ieki R, Saitoh E, Shibuya M. Acute lung injury as a possible adverse drug reaction related to gefitinib. Eur Respir J 2003;22:179–81.
[4] Okamoto I, Fujii K, Matsumoto M, et al. Diffuse alveolar damage after ZD1839 therapy in a patient with non-small cell lung cancer. Lung Cancer 2003;40:339–42.
[5] Sumpter K, Harper-Wynne C, O'Brien M. Severe acute interstitial pneumonia and gefitinib. Lung Cancer 2004;43:367–8.
[6] Ohyanagi F, Ando Y, Nagashima F, et al. Acute gefitinib-induced pneumonitis. Int J Clin Oncol 2004;9:406–9.
[7] Sakai F, Kusumoto M, Johkoh T et al. CT findings of lung damage induced by gefitinib (Iressa™) in 37 patients. Personal communication; 2005.
[8] Expert Committee Meeting Report. Final report on interstitial lung disease (ILD) related to gefitinib (Iressa Tablet 250) by Iressa Expert Committee. AstraZeneca, March 26, 2003.
[9] Padley SPG, Adler B, Hansell DM, et al. High-resolution computed tomography of drug-induced lung disease. Clin Radiol 1992;46:232–6.
[10] Akira M, Ishikawa H, Yamamoto S. Drug-induced pneumonitis: thin-section CT findings in 60 patients. Radiology 2002;224:852–60.
[11] Erasmus JJ, McAdams HP, Rossi SE. High-resolution CT of drug-induced lung disease. Radiol Clin North Am 2002;40:61–72.
[12] Cleverly JR, Screaton NJ, Hiors MP, et al. Drug-induced lung disease: high-resolution CT and histological findings. Clin Radiol 2002;57:292–9.
[13] Pieta GG. Pathologic mechanisms of drug-induced lung disorders. J Thorac Imag 1991;61:1–7.
[14] Ichikado K, Suga M, Muller NL, et al. Acute interstitial pneumonia: comparison of high-resolution computed tomography findings between survivors and nonsurvivors. Am J Respir Crit Care Med 2002;165:1551–6.
[15] Takano T, Ohe Y, Kusumoto M, et al. Risk factors for interstitial lung disease and predictive factors for tumor response in patients with advanced non-small cell lung cancer treated with gefitinib. Lung Cancer 2004;45:93–104.

Biochem. J. (2006) 397, 537–543 (Printed in Great Britain) doi:10.1042/BJ20051962

In-frame deletion in the EGF receptor alters kinase inhibition by gefitinib

Kazuko SAKAI*†, Hideyuki YOKOTE‡, Kimiko MURAKAMI-MUROFUSHI†, Tomohide TAMURA§, Nagahiro SAIJO§ and Kazuto NISHIO*‡[1]

*Shien-Lab, National Cancer Center Research Institute, Tsukiji 5-1-1, Chuo-ku, Tokyo 104-0045, Japan, †Department of Biology, Faculty of Science, Ochanomizu University, 2-1-1 Ohtsuka, Tokyo 112-8610, Japan, ‡Pharmacology Division, National Cancer Center Research Institute, Tsukiji 5-1-1, Chuo-ku, Tokyo 104-0045, Japan, and §Medical Oncology, National Cancer Center Hospital, National Cancer Center Research Institute, Tsukiji 5-1-1, Chuo-ku, Tokyo 104-0045, Japan

The existence of an in-frame deletion mutant correlates with the sensitivity of lung cancers to EGFR (epidermal growth factor receptor)-targeted tyrosine kinase inhibitors. We reported previously that the in-frame 15-bp deletional mutation (delE746–A750 type deletion) was constitutively active in cells. Kinetic parameters are important for characterizing an enzyme; however, it remains unclear whether the kinetic parameters of deletion mutant EGFR are similar to those of wild-type EGFR. We analysed autophosphorylation in response to ATP and inhibition of gefitinib for deletion mutant EGFR and wild-type EGFR. Kinetic studies, examining autophosphorylation, were carried out using EGFR fractions extracted from 293-pΔ15 and 293-pEGFR cells transfected with deletion mutant EGFR and wild-type EGFR respectively. We demonstrated the difference in activities between unstimulated wild-type (K_m for ATP $= 4.0 \pm 0.3$ μM) and mutant EGFR (K_m for ATP $= 2.5 \pm 0.2$ μM). There was no difference in K_m values between EGF-stimulated wild-type EGFR (K_m for ATP $= 1.9 \pm 0.1$ μM) and deletion mutant EGFR (K_m for ATP $= 2.2 \pm 0.2$ μM). These results suggest that mutant EGFR is active without ligand stimulation. The K_i value for gefitinib of the deletion mutant EGFR was much lower than that of wild-type EGFR. These results suggest that the deletion mutant EGFR has a higher affinity for gefitinib than wild-type EGFR.

Key words: autophosphorylation, epidermal growth factor receptor (EGFR), gefitinib, kinase inhibition, tyrosine kinase.

INTRODUCTION

EGFR [EGF (epidermal growth factor) receptor] is among the most important targets for lung cancer therapy, and many EGFR-targeted inhibitors have been developed [1]. These EGFR-targeted compounds inhibit the tyrosine kinase activity of EGFR by competing at the ATP-binding site [2]. Many EGFR-targeted tyrosine kinase inhibitors such as gefitinib and erlotinib have been assessed clinically [3,4]. Recently, an EGFR mutation was found in patients who responded to gefitinib, and mutant EGFR has been reported to be a determinant of the response to EGFR tyrosine kinase inhibitors [5,6]. To date, over 30 EGFR mutations including delE746–A750, L858R and delL747–P753insS, have been reported in lung cancer. These EGFR mutations, except for T790M, are considered to be of the 'gain-of-function' type. Differences exist among them; for example, constitutively active in delE746–A750 compared with hyperresponsive to ligand stimulation in L858R and delL747–P753insS, although these mutant EGFRs increase sensitivity to EGFR-targeted tyrosine kinase inhibitors [7–9]. In general, the observation of hyperresponsiveness to ligand stimulation, as in the case of L858R, raises the possibility of high affinity for ATP. We reported previously that deletion mutant EGFR was constitutively phosphorylated under unstimulated conditions, whereas wild-type EGFR was not phosphorylated until ligand stimulation [7]. The differences in cellular phenotype and sensitivity to gefitinib between deletion mutant EGFR and wild-type EGFR raise the possibility that the enzymatic properties of the deletion mutant EGFR may differ from those of wild-type EGFR. However, it remains unclear whether the kinetic parameters of deletion mutant EGFR are different from those of wild-type EGFR. In the present study, we focused on the autophosphorylation of deletion mutant EGFR, and investigated the inhibition constant of gefitinib. Technically, we used deletion mutant EGFR and wild-type EGFR extracted from ectopically expressed HEK-293 (human embryonic kidney) cells. The autophosphorylation assay reflects the native behaviour of EGFR in maintaining cellular functions.

MATERIALS AND METHODS

Reagents

Gefitinib (Iressa®, ZD1839) was provided by AstraZeneca.

Cell culture

The HEK-293 cell line was obtained from the A.T.C.C. (Manassas, VA, U.S.A.) and was cultured in RPMI 1640 medium (Sigma) supplemented with 10% heat-inactivated foetal bovine serum (Life Technologies).

Plasmid construction and transfection

Construction of the expression plasmid vector of wild-type EGFR and the 15-bp deletion mutant EGFR (delE746–A750 type deletion), which has the same deletion site as that observed in detail in PC-9 cells, has been described elsewhere [7,10,11]. The plasmids were transfected into HEK-293 cells and the transfectants were selected using Zeosin (Sigma). The stable transfectants (pooled cultures) of the wild-type EGFR and its deletion mutant were designated 293-pEGFR and 293-pΔ15 cells respectively.

Abbreviations used: EGF, epidermal growth factor; EGFR, EGF receptor; HEK-293, human embryonic kidney; 293-pEGFR, HEK-293 cells transfected with wild-type EGFR; 293-pΔ15, HEK-293 cells transfected with deletion mutant EGFR; TBS-T, Tris-buffered saline with Tween 20; TGF-α, transforming growth factor-α.

[1] To whom correspondence should be addressed (email knishio@gan2.res.ncc.go.jp).

Immunoblotting

The 293-pΔ15 and 293-pEGFR cells were treated with or without gefitinib for 3 h, stimulated with EGF (100 ng/ml) under serum-starvation conditions and then lysed for immunoblot analysis. Immunoblot analysis was performed as described previously [12]. Equivalent amounts of protein were separated by SDS/PAGE (2–15 % gradient) and transferred to a PVDF membrane (Millipore). The membrane was probed with a mouse monoclonal antibody against EGFR (Transduction Laboratories), a phospho-EGFR antibody (specific for Tyr^{1068}) (Cell Signaling Technology) as the first antibody, followed by a horseradish-peroxidase-conjugated secondary antibody. The bands were visualized with ECL® (enhanced chemiluminescence) (Amersham Biosciences).

Determination of ligand secretion by ELISA

The 293-pΔ15 and 293-pEGFR cells were cultured in 12-well plates under serum-starvation conditions. The cell culture supernatant was collected for each cell line and stored at −80 °C for further analysis. Amounts of EGF and TGF-α (transforming growth factor α) in the culture medium from each cell line were determined with a DuoSet ELISA development kit (R&D Systems). The assay was performed in triplicate according to the manufacturer's instructions.

Preparation of cell lysates for EGFR autophosphorylation

Cultivated cells, after reaching 70–80 % confluence, were starved in serum-free medium for 24 h, with or without EGF (100 ng/ml) stimulation. The cells were washed twice with ice-cold PBS containing 0.33 mM $MgCl_2$ and 0.9 mM $CaCl_2$ [PBS(+)], then lysed with lysis buffer [50 mM Tris/HCl, pH 7.4, 50 mM NaCl, 0.25 % Triton X-100, 5 mM EDTA, protease inhibitor (Roche Diagnostics) and phosphatase inhibitor (Sigma)]. For the preparation of gefitinib-treated cell lysates, cultivated cells were starved in serum-free medium for 24 h, and were then pre-incubated with 2 μM gefitinib for 3 h. Either with or without EGF stimulation (100 ng/ml), the cells were washed twice with ice-cold PBS(+) and lysed with lysis buffer. The cell lysate was centrifuged at 20000 *g* for 10 min, and the protein concentration of the supernatant was measured with a BCA (bicinchoninic acid) protein assay (Pierce).

Autophosphorylation assay

The amount of EGFR in 293-pΔ15 and 293-pEGFR cells was determined by quantitative immunoassay (R&D Systems) according to the manufacturer's instructions. The autophosphorylation assay was carried out with a quantitative immunoassay system. Wells in a 96-well immunomodule (Nalge Nunc International) were incubated with 0.8 μg/ml goat anti-(human EGFR) antibody in PBS (provided with the EGFR quantitative immunoassay system) and incubated at 4 °C overnight. The plates were washed three times with TBS-T (Tris-buffered saline with Tween 20; 20 mM Tris/HCl, pH 7.4, 150 mM NaCl and 0.05 % Tween 20) and were then filled with blocking buffer (PBS containing 1 % BSA and 5 % sucrose) and incubated for 2 h at room temperature (25 °C). The wells were washed three times with TBS-T and incubated with cell lysates of 293-pEGFR or 293-pΔ15 including equal amounts of EGFR (130 ng of EGFR/well) diluted with lysis buffer. After a 2 h incubation at room temperature, the 96-well plate was washed with TBS-T. Autophosphorylation of EGFR was initiated by addition of ATP (0–32 μM in 50 mM Tris/HCl, pH 7.5, 20 mM $MgCl_2$ and phosphatase inhibitor) followed by incubation for 5 min. In some experiments, various concentrations of gefitinib were added to the wells before the addition of ATP. Following the autophosphorylation reaction, the wells were washed with TBS-T. Next,

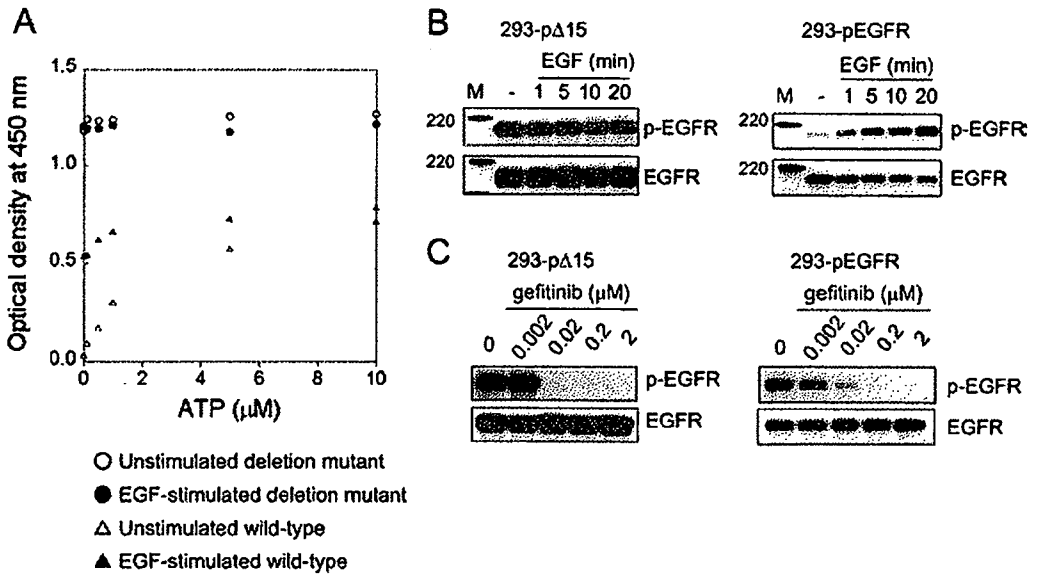

Figure 1 Autophosphorylation reactions of deletion mutant EGFR and wild-type EGFR

(**A**) The 293-pΔ15 and 293-pEGFR cells were treated with or without EGF (100 ng/ml) for 10 min after serum-starvation. EGFR was extracted from the cells and immobilized on wells with anti-EGFR antibody. Autophosphorylation reactions were initiated by the addition of ATP, and autophosphorylation was detected using horseradish-peroxidase-conjugated phosphotyrosine antibody, measuring the absorbance ('optical density') at 450 nm. Autophosphorylation was seen for unstimulated (○) and EGF-stimulated (●) deletion mutant EGFR, and unstimulated (△) and EGF-stimulated (▲) wild-type EGFR. Results are representative of at least three independent experiments. (**B**) The 293-pΔ15 and 293-pEGFR cells were treated with or without EGF (100 ng/ml) for the indicated times after serum-starvation. Phosphorylation of EGFR and total EGFR was determined by immunoblotting. (**C**) The 293-pΔ15 and 293-pEGFR cells were exposed to gefitinib (0.002–2 μM) for 3 h under serum-starvation conditions, and stimulated with EGF (100 ng/ml) for 10 min. The cells were then lysed and subjected to immunoblot analysis.

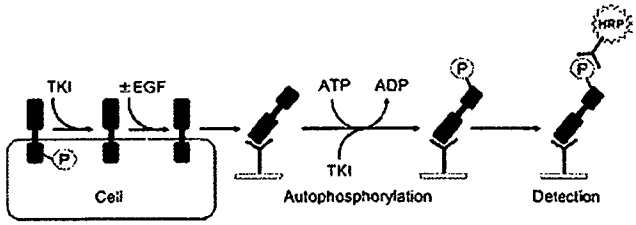

Figure 2 Schematic illustration of the cell-based autophosphorylation assay

The 293-pΔ15 and the 293-pEGFR cells overexpressing deletion mutant EGFR and wild-type EGFR respectively were treated with 2 μM gefitinib for 3 h and stimulated with or without EGF (100 ng/ml) under serum-starvation conditions. EGFR was extracted from cells and immobilized on wells with anti-EGFR antibody. The autophosphorylation reaction was initiated by the addition of ATP with or without gefitinib, and horseradish-peroxidase-conjugated anti-phosphotyrosine antibody was used to detect the phosphorylation of EGFR. TKI, tyrosine kinase inhibitor.

horseradish-peroxidase-conjugated anti-phosphotyrosine antibody, PY-99-HRP (0.4 μg/ml in PBS containing 1% BSA and 0.1% Tween 20) (Santa Cruz Biotechnology) was added to the wells for 2 h at room temperature. The wells were washed three times with TBS-T. Bound phosphotyrosine antibody was detected colorimetrically after adding 100 μl of substrate (tetramethylbenzidine and H_2O_2) to each well. After a 10 min incubation, the colour reaction was quenched by the addition of 100 μl of 1M H_2SO_4. The absorbance readings for each well were determined at 450 nm with Delta-soft on an Apple Macintosh computer interfaced to a Bio-Tek Microplate Reader EL-340 (BioMetallics).

Data analysis

For kinetic analysis, an Eadie–Hofstee plot was applied for the calculation of K_m (Michaelis constant) and V_{max} (maximum velocity). The data obtained were plotted as velocity against velocity/substrate concentration (V/ATP). The slope of the line is equal to $-K_m$ and the x-intercept is V_{max}. The K_i value was calculated as follows:

$$K_i = (K_m \times [I])/(K_{m,I} - K_m) \quad (1)$$

in which K_m is the Michaelis constant for ATP, $K_{m,I}$ is the Michaelis constant for ATP in the presence of gefitinib and [I] is the concentration of gefitinib. The statistical analysis was performed using KaleidaGraph (Synergy Software).

RESULTS

Autophosphorylation of deletion mutant EGFR and wild-type EGFR

We performed the autophosphorylation assay and immunoblot analysis using lysates extracted from 293-pΔ15 and 293-pEGFR cells under unstimulated and EGF-stimulated conditions (Figures 1A and 1B). Under unstimulated conditions, deletion mutant EGFR was highly phosphorylated in the absence of ATP. Addition of ATP did not affect the autophosphorylation of deletion mutant EGFR. On the other hand, autophosphorylation of wild-type EGFR was barely detectable without ATP, and proceeded in an ATP-dependent manner. In the EGF-stimulated case, wild-type EGFR was phosphorylated to a greater extent in the absence of ATP than unstimulated wild-type EGFR. The autophosphorylation of EGF-stimulated wild-type EGFR additively increased with the addition of ATP. These findings indicate that the deletion mutant retains the constitutive activity in our autophosphorylation assay. In the immunoblot analysis, phosphorylation of deletion mutant EGFR was detected in 293-pΔ15 cells without ligand stimulation. Addition of EGF increased phosphorylation of EGFR in the 293-pEGFR cells. Taken together, these results indicate that the deletion mutant has constitutive autophosphorylation activity.

In addition, we examined the secretion of major ligands for EGFR such as EGF and TGF-α from transfected HEK-293 cells by ELISA. No detectable EGF and TGF-α secretion was observed in the cultivation medium used for HEK-293 transfectants (results not shown), indicating that these transfectants are not activated via EGF-mediated autocrine loops. We considered that autophosphorylation using unstimulated EGFR represents a

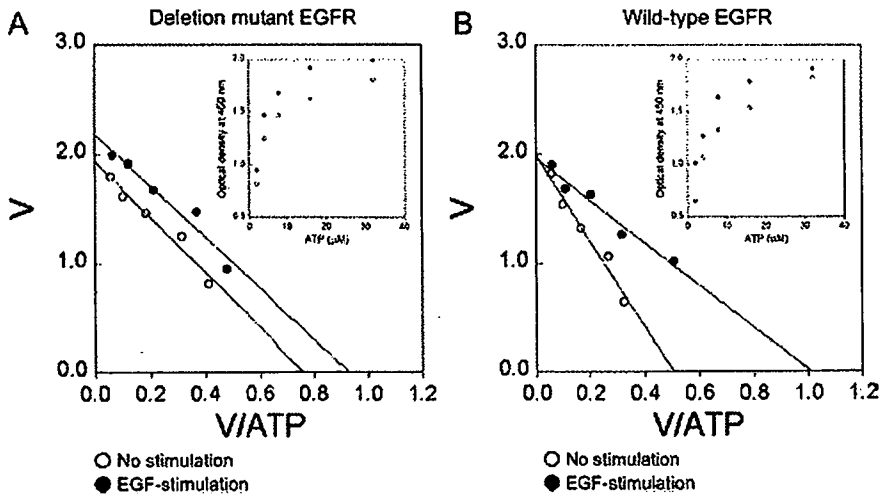

Figure 3 Autophosphorylation activities of deletion mutant EGFR and wild-type EGFR

Plots of absorbance ('optical density') against ATP concentration (inset) were fitted to an Eadie–Hofstee plot to calculate the values of kinetic parameters (K_m and V_{max}) for deletion mutant EGFR (A) and wild-type EGFR (B) under unstimulated (O) and EGF-stimulated conditions (●). Results are representative of at least three independent experiments with similar results.

Table 1 Kinetic parameters for ATP

The autophosphorylation reaction was performed using the indicated enzyme and gefitinib (0.5–5 nM). The steady-state kinetic parameters for ATP were determined from the Eadie–Hofstee plot in Figure 5. Results are means ± S.D. for three independent duplicate experiments.

		K_m (μM)				V_{max} (μM · min^{-1})			
		Deletion mutant		Wild-type		Deletion mutant		Wild-type	
Gefitinib (nM)	EGF stimulation...	−	+	−	+	−	+	−	+
0		2.5 ± 0.2	2.2 ± 0.2	4.0 ± 0.3	1.9 ± 0.1	1.9 ± 0.1	2.1 ± 0.1	2.0 ± 0.0	1.9 ± 0.0
0.5		5.6 ± 0.5	5.7 ± 0.4	4.1 ± 0.4	2.3 ± 0.1	1.9 ± 0.1	1.9 ± 0.2	2.0 ± 0.1	1.9 ± 0.1
1		9.8 ± 2.8	10.9 ± 3.0	4.6 ± 1.2	2.5 ± 0.1	2.0 ± 0.1	1.9 ± 0.0	2.0 ± 0.2	1.8 ± 0.1
5		26.1 ± 5.4	30.2 ± 4.2	7.0 ± 2.3	4.9 ± 0.9	1.9 ± 0.1	1.8 ± 0.2	2.0 ± 0.1	1.8 ± 0.2

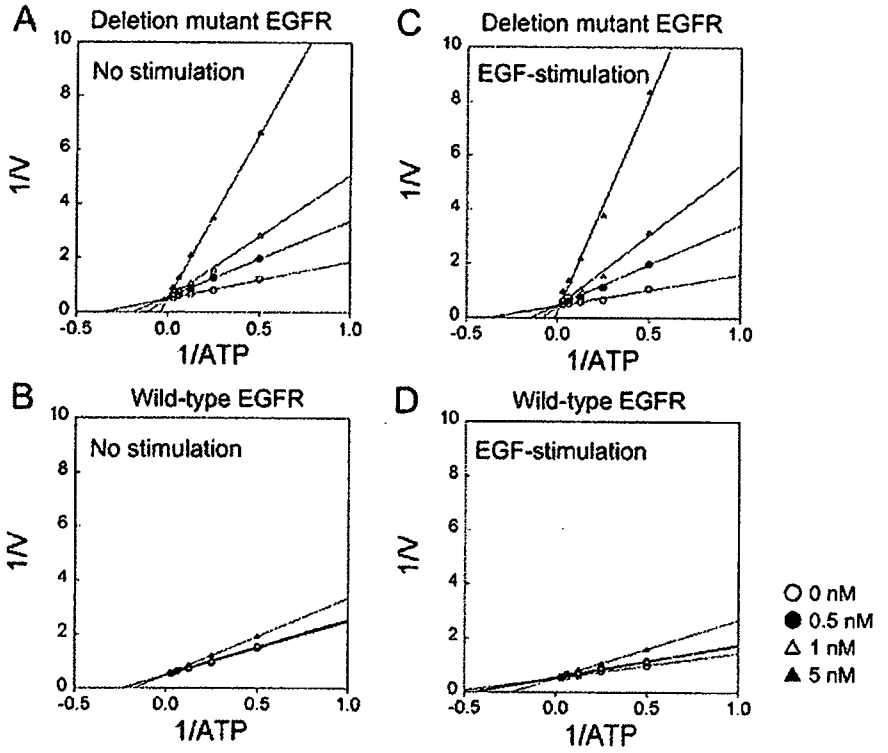

Figure 4 Mechanism of inhibition of deletion mutant EGFR by gefitinib

Autophosphorylation of unstimulated deletion mutant (**A**), unstimulated wild-type (**B**), EGF-stimulated deletion mutant (**C**) and EGF-stimulated wild-type (**D**) EGFR was measured with or without gefitinib at concentrations of 0 (○), 0.5 (●), 1 (△) and 5 (▲) nM. Reciprocal velocity against reciprocal ATP concentrations (0.5–32 μM) were plotted. Data are representative of at least three independent experiments.

low level of EGF-independent basal phosphorylation, whereas autophosphorylation using EGF-stimulated EGFR represents EGF-induced phosphorylation.

Kinetic parameters of autophosphorylation

The deletion mutant EGFR is constitutively phosphorylated under unstimulated conditions. Measuring the autophosphorylation activity of deletion mutant EGFR requires unphosphorylated tyrosine residues of EGFR. An autophosphorylation assay was reconstructed to determine the kinetic parameters of deletion mutant EGFR. The method is summarized in Figure 2. The concentrations of gefitinib used (2 μM) completely inhibited phosphorylation of both the deletion mutant and wild-type EGFR, as demonstrated by immunoblot analysis (Figure 1C). We performed autophosphorylation assays with various amounts of EGFR (results not shown). In our autophosphorylation assay, a constant amount of EGFR (130 ng/well) was adopted to measure its autophosphorylation, because this amount of EGFR was found to be appropriate for detecting changes in the absorbance of both wild-type and deletion mutant EGFR. The autophosphorylation of deletion mutant EGFR and wild-type EGFR was analysed by comparison with unstimulated and EGF-stimulated EGFR (Figure 3). The higher phosphorylation of deletion mutant EGFR shown in Figure 1(A) was lowered by using gefitinib-treated lysates, while the autophosphorylation reaction was initiated by addition of ATP. The ATP-dependent autophosphorylation reactions of deletion mutant EGFR and wild-type EGFR in crude cellular extracts were monitored (Figure 3, insets). The data were transformed into an Eadie–Hofstee plot, and the kinetic parameters were determined as apparent K_m and V_{max} values for ATP (Figure 3 and Table 1). Under unstimulated conditions,

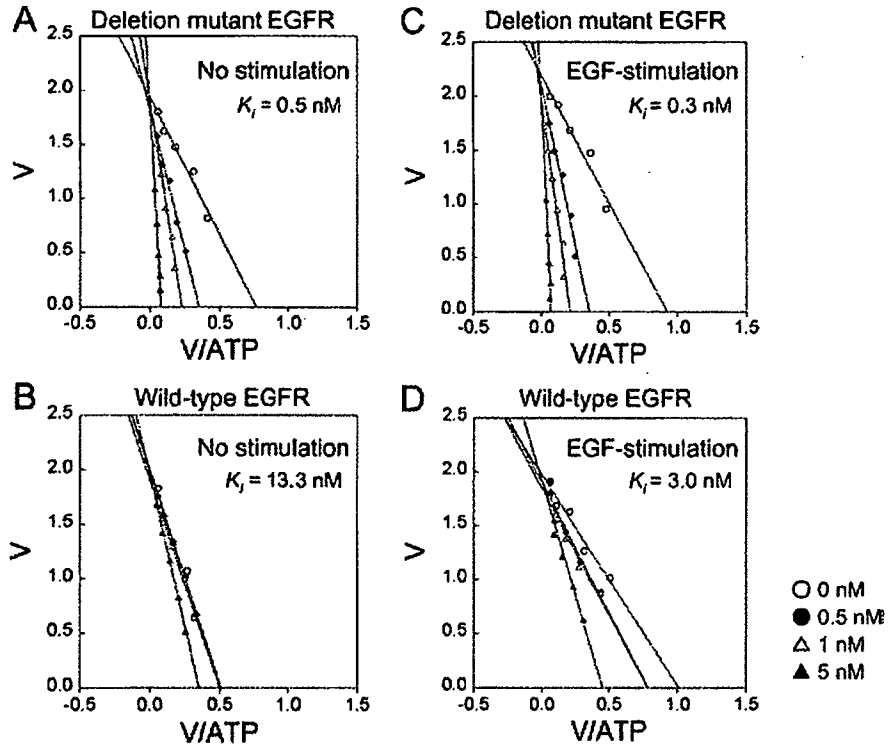

Figure 5 Inhibition constant of gefitinib for autophosphorylation activity of deletion mutant EGFR

The same dataset as shown in Figure 4 was fitted to an Eadie–Hofstee plot, and kinetic parameters from this fit are summarized in Table 1. Shown are the results for the unstimulated (**A**) and EGF-stimulated (**C**) deletion mutant EGFR and unstimulated (**B**) and EGF-stimulated (**D**) wild-type EGFR in response to ATP with or without gefitinib at concentrations of 0 (○), 0.5 (●), 1 (△) and 5 (▲) nM. Results are representative of at least three independent experiments.

differences in activities were seen between unstimulated wild-type (K_m for ATP = 4.0 ± 0.3 μM) and deletion mutant EGFR (K_m for ATP = 2.5 ± 0.2 μM). Under EGF-stimulated conditions, there was no difference in K_m values between EGF-stimulated wild-type EGFR (K_m for ATP = 1.9 ± 0.1 μM) and deletion mutant EGFR (K_m for ATP = 2.2 ± 0.2 μM). The V_{max} values of wild-type EGFR and deletion mutant EGFR were equal under both conditions. These results suggest that the wild-type EGFR is conformationally activated by EGF stimulation, and that the mutant EGFR is active without ligand stimulation.

Gefitinib inhibits autophosphorylation of deletion mutant EGFR

We examined the inhibitory effect of gefitinib (0.5, 1 and 5 nM) on the autophosphorylation of deletion mutant EGFR in comparison with wild-type EGFR under unstimulated and EGF-stimulated conditions. The data were transformed into a Lineweaver–Burk plot for estimation of the mode of inhibition (Figure 4). Lineweaver–Burk plot analysis showed that gefitinib competitively inhibited the autophosphorylation of deletion mutant EGFR as well as that of wild-type EGFR. The data were transformed into an Eadie–Hofstee plot for determination of kinetic parameters (Figure 5). Eadie–Hofstee plot analysis revealed the apparent K_m and V_{max} values for ATP in the presence of various gefitinib concentrations, and the kinetic parameters are summarized in Table 1. The K_i for deletion mutant EGFR and wild-type EGFR was calculated using eqn 1 (see the Materials and methods section). The K_i value of gefitinib for deletion mutant EGFR (K_i for gefitinib = 0.5 ± 0.1 nM) was 26-fold lower than that for wild-type EGFR (K_i for gefitinib = 13.3 ± 5.1 nM) under unstimulated conditions (Figure 5). Under EGF-stimulated conditions, the K_i value of gefitinib for deletion mutant EGFR (0.3 ± 0.1 nM) was 10-fold lower than that for wild-type EGFR (3.0 ± 0.6 nM) (Figure 5). Based on these comparative studies, we concluded that gefitinib binds deletion mutant EGFR more strongly than wild-type EGFR. In addition, we calculated the inhibitory effect of gefitinib for both types of EGFR in the presence of 2 μM ATP (Figure 6). Relatively strong inhibitory activity was detected for deletion mutant EGFR as compared with wild-type EGFR. These results suggest that gefitinib had a high affinity (low K_i value) for deletion mutant EGFR compared with wild-type EGFR.

DISCUSSION

Wild-type EGFR is unphosphorylated, being in an inactive form, under unstimulated conditions. The binding of ligands to the extracellular domain of EGFR induces dimerization and phosphorylation of the receptor into the active form [13]. The kinetic parameters of wild-type EGFR in our autophosphorylation assay are consistent with those of previous reports [14,15]. Crystallographic analysis has shown that the structure of the EGFR kinase domain after forming a complex with erlotinib exhibits a conformation consistent with the active form of protein kinases [16,17]. Previously, we reported that the deletion mutant EGFR was dimerized and phosphorylated constitutively without ligand stimulation, suggesting an active conformation [9]. We analysed the enzymatic properties of the deletion mutant EGFR, and

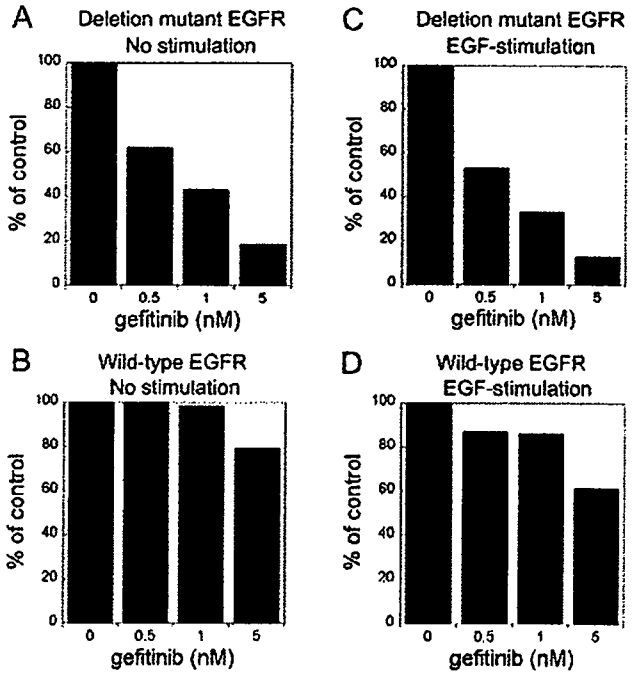

Figure 6 Effects of gefitinib on autophosphorylation of deletion mutant EGFR

The percentage of absorbance compared with the control under conditions of 2 μM ATP was calculated using the same dataset as shown in Figure 4 at a concentration of 2 μM ATP. The results shown are for unstimulated (**A**) and EGF-stimulated (**C**) deletion mutant EGFR and unstimulated (**B**) and EGF-stimulated (**D**) wild-type EGFR in response to ATP with or without gefitinib. Results are representative of at least three independent experiments.

determined the K_i value of gefitinib for deletion mutant EGFR. The inhibition constant of gefitinib for wild-type EGFR was similar to the value reported by Wakeling et al. [18]. We showed that the K_i value of gefitinib for deletion mutant EGFR was much lower than that for wild-type EGFR. The evidence of the decreased K_i value of gefitinib for deletion mutant EGFR means that gefitinib binds deletion mutant EGFR more strongly than wild-type EGFR. The high-affinity interaction between deletion mutant EGFR and gefitinib may be attributable to structural differences between deletion mutant EGFR and wild-type EGFR.

Our conclusion does not contradict the previous report by Stamos et al. [16] on a similar EGFR-targeted tyrosine kinase inhibitor, erlotinib, which binds to the active form of EGFR [14]. This result differs from that reported elsewhere: Fabian et al. [19] reported that there were no differences in the binding affinity of EGFR-targeted tyrosine kinase inhibitors between wild-type EGFR and mutant EGFR, including the deletion mutation. They constructed and expressed the kinase domain of EGFR on a bacteriophage surface, followed by interaction with immobilized inhibitors using biotin–avidin systems. Conversely, in our experiments, we performed autophosphorylation assays with EGFR extracted from 293-pΔ15 and the 293-pEGFR cells overexpressing deletion mutant and wild-type EGFR respectively. We consider our cell-based autophosphorylation assay results to reflect the native state of deletion mutant EGFR and to possibly explain the hypersensitivity of mutant-expressing cells to gefitinib.

We demonstrated that the deletion mutant actually binds gefitinib more strongly than wild-type EGFR. This is likely to be the mechanism of action of other tyrosine kinase inhibitors such as erlotinib, ZD6474 [dual inhibitor targeted to VEGFR2 (vascular endothelial growth factor receptor 2)/KDR (kinase insert domain-containing receptor) and EGFR] and other possible multi-targeted tyrosine kinase inhibitors. Indeed, EGFR-specific tyrosine kinase inhibitors AG1478 and erlotinib, as well as ZD6474, as described in our previous report [7] showed different growth-inhibitory activities against HEK-293 transfected with deletion mutant EGFR (results not shown). Thus it is likely that these (ATP competitive) tyrosine kinase inhibitors have different binding property effects on wild-type and deletion mutant EGFR to those of gefitinib.

In the present study, we focused on the enzymatic properties of in-frame deletion mutant EGFR (delE746–A750). The inhibition of receptor autophosphorylation in deletion mutant EGFR by gefitinib was much greater than that in wild-type EGFR. Next, it is necessary to examine the kinetic properties of other types of EGFR mutants, especially L858R, and these findings may pave the way for the discovery of different kinase inhibitors with different inhibition profiles for EGFR.

This work was supported by funds for the Third Term Comprehensive 10-Year Strategy for Cancer Control.

REFERENCES

1 Arteaga, C. L. (2003) ErbB-targeted therapeutic approaches in human cancer. Exp. Cell Res. **284**, 122–130
2 Traxler, P., Furet, P., Mett, H., Buchdunger, E., Meyer, T. and Lydon, N. (1997) Design and synthesis of novel tyrosine kinase inhibitors using a pharmacophore model of the ATP-binding site of the EGF-R. J. Pharm. Belg. **52**, 88–96
3 Shepherd, F. A., Rodrigues Pereira, J., Ciuleanu, T., Tan, E. H., Hirsh, V., Thongprasert, S., Campos, D., Maoleekoonpiroj, S., Smylie, M., Martins, R. et al. (2005) Erlotinib in previously treated non-small-cell lung cancer. N. Engl. J. Med. **353**, 123–132
4 Bell, D. W., Lynch, T. J., Haserlat, S. M., Harris, P. L., Okimoto, R. A., Brannigan, B. W., Sgroi, D. C., Muir, B., Riemenschneider, M. J., Iacona, R. B. et al. (2005) Epidermal growth factor receptor mutations and gene amplification in non-small-cell lung cancer: molecular analysis of the IDEAL/INTACT gefitinib trials. J. Clin. Oncol. **23**, 8081–8092
5 Lynch, T. J., Bell, D. W., Sordella, R., Gurubhagavatula, S., Okimoto, R. A., Brannigan, B. W., Harris, P. L., Haserlat, S. M., Supko, J. G., Haluska, F. G. et al. (2004) Activating mutations in the epidermal growth factor receptor underlying responsiveness of non-small-cell lung cancer to gefitinib. N. Engl. J. Med. **350**, 2129–2139
6 Paez, J. G., Janne, P. A., Lee, J. C., Tracy, S., Greulich, H., Gabriel, S., Herman, P., Kaye, F. J., Lindeman, N., Boggon, T. J. et al. (2004) EGFR mutations in lung cancer: correlation with clinical response to gefitinib therapy. Science **304**, 1497–1500
7 Arao, T., Fukumoto, H., Takeda, M., Tamura, T., Saijo, N. and Nishio, K. (2004) Small in-frame deletion in the epidermal growth factor receptor as a target for ZD6474. Cancer Res. **64**, 9101–9104
8 Tracy, S., Mukohara, T., Hansen, M., Meyerson, M., Johnson, B. E. and Janne, P. A. (2004) Gefitinib induces apoptosis in the EGFRL858R non-small-cell lung cancer cell line H3255. Cancer Res. **64**, 7241–7244
9 Sakai, K., Arao, T., Shimoyama, T., Murofushi, K., Sekijima, M., Kaji, N., Tamura, T., Saijo, N. and Nishio, K. (2005) Dimerization and the signal transduction pathway of a small in-frame deletion in the epidermal growth factor receptor. FASEB J. **20**, 311–313
10 Nishio, K., Arioka, H., Ishida, T., Fukumoto, H., Kurokawa, H., Sata, M., Ohata, M. and Saijo, N. (1995) Enhanced interaction between tubulin and microtubule-associated protein 2 via inhibition of MAP kinase and CDC2 kinase by paclitaxel. Int. J. Cancer **63**, 688–693
11 Kawamura-Akiyama, Y., Kusaba, H., Kanzawa, F., Tamura, T., Saijo, N. and Nishio, K. (2002) Non-cross resistance of ZD0473 in acquired cisplatin-resistant lung cancer cell lines. Lung Cancer **38**, 43–50
12 Koizumi, F., Shimoyama, T., Taguchi, F., Saijo, N. and Nishio, K. (2005) Establishment of a human non-small cell lung cancer cell line resistant to gefitinib. Int. J. Cancer **116**, 36–44
13 Tanner, K. G. and Kyte, J. (1999) Dimerization of the extracellular domain of the receptor for epidermal growth factor containing the membrane-spanning segment in response to treatment with epidermal growth factor. J. Biol. Chem. **274**, 35985–35990
14 Nair, N., Davis, R. J. and Robinson, H. L. (1992) Protein tyrosine kinase activities of the epidermal growth factor receptor and ErbB proteins: correlation of oncogenic activation with altered kinetics. Mol. Cell. Biol. **12**, 2010–2016

15 Wood, E. R., Truesdale, A. T., McDonald, O. B., Yuan, D., Hassell, A., Dickerson, S. H., Ellis, B., Pennisi, C., Horne, E., Lackey, K. et al. (2004) A unique structure for epidermal growth factor receptor bound to GW572016 (Lapatinib): relationships among protein conformation, inhibitor off-rate, and receptor activity in tumor cells. Cancer Res. **64**, 6652–6659
16 Stamos, J., Sliwkowski, M. X. and Eigenbrot, C. (2002) Structure of the epidermal growth factor receptor kinase domain alone and in complex with a 4-anilinoquinazoline inhibitor. J. Biol. Chem. **277**, 46265–46272
17 Noble, M. E., Endicott, J. A. and Johnson, L. N. (2004) Protein kinase inhibitors: insights into drug design from structure. Science **303**, 1800–1805
18 Wakeling, A. E., Guy, S. P., Woodburn, J. R., Ashton, S. E., Curry, B. J., Barker, A. J. and Gibson, K. H. (2002) ZD1839 (Iressa): an orally active inhibitor of epidermal growth factor signaling with potential for cancer therapy. Cancer Res. **62**, 5749–5754
19 Fabian, M. A., Biggs, 3rd, W. H., Treiber, D. K., Atteridge, C. E., Azimioara, M. D., Benedetti, M. G., Carter, T. A., Ciceri, P., Edeen, P. T., Floyd, M. et al. (2005) A small molecule-kinase interaction map for clinical kinase inhibitors. Nat. Biotechnol. **23**, 329–336

Received 12 December 2005/3 April 2006; accepted 20 April 2006
Published as BJ Immediate Publication 20 April 2006, doi:10.1042/BJ20051962

Jpn J Clin Oncol 2006;36(5)269–273
doi:10.1093/jjco/hyl021

Interstitial Shadow on Chest CT is Associated with the Onset of Interstitial Lung Disease Caused by Chemotherapeutic Drugs

Seiji Niho, Koichi Goto, Kiyotaka Yoh, Young Hak Kim, Hironobu Ohmatsu, Kaoru Kubota, Nagahiro Saijo and Yutaka Nishiwaki

Division of Thoracic Oncology, National Cancer Center Hospital East, Chiba, Japan

Received October 10, 2005; accepted February 8, 2006; published online May 15, 2006

Objective: Pretreatment computerized tomography (CT) films of the chest was studied to clarify the influence of interstitial shadow on developing interstitial lung disease (ILD).
Methods: Eligible patients were those lung cancer patients who started to receive first-line chemotherapy between October 2001 and March 2004. Patients who received thoracic radiotherapy to the primary lesion, mediastinum, spinal or rib metastases were excluded. We reviewed pretreatment conventional CT and plain X-ray films of the chest. Ground-glass opacity, consolidation or reticular shadow without segmental distribution was defined as interstitial shadow, with this event being graded as mild, moderate or severe. If interstitial shadow was detected on CT films of the chest, but not via plain chest X-ray, it was graded as mild. Patients developing ILD were identified from medial records.
Results: A total of 502 patients were eligible. Mild, moderate and severe interstitial shadow was identified in 7, 8 and 5% of patients, respectively. A total of 188 patients (37%) received tyrosine kinase inhibitor (TKI) treatment, namely gefitinib or erlotinib. Twenty-six patients (5.2%) developed ILD either during or after chemotherapy. Multivariate analyses revealed that interstitial shadow on CT films of the chest and treatment history with TKI were associated with the onset of ILD.
Conclusions: It is recommended that patients with interstitial shadow on chest CT are excluded from future clinical trials until this issue is further clarified, as it is anticipated that use of chemotherapeutic agents frequently mediate onset of ILD in this context.

Key words: interstitial lung disease – interstitial shadow – chemotherapy – lung cancer – CT

INTRODUCTION

Interstitial lung disease (ILD) is known to be an adverse event in cancer chemotherapy and radiotherapy. Recently, ILD has attracted considerable attention in Japan since the observation that gefitinib caused ILD (1). Gefitinib is a tyrosine kinase inhibitor (TKI) of epidermal growth factor receptor and is active in patients with recurrent non-small cell lung cancer (NSCLC) after platinum-based chemotherapy (2,3). Gefitinib was first approved for the treatment of advanced NSCLC by the Japanese regulatory agencies on 5 July 2002. From August 2002 to April 2003, ~28 000 patients with NSCLC were given gefitinib in Japan. However, 616 patients suffered from ILD and 246 patients died of ILD, according to a report from AstraZeneca. The West Japan Thoracic Oncology Group conducted a retrospective survey to clarify the risk factors related to ILD (4). Out of 1976 patients with NSCLC who received gefitinib across 84 institutions, 91 patients were suspected of having developed ILD. This group also analyzed the patients' background, together with computerized tomography (CT) films of the chest, before treatment and at the onset of ILD in this subcohort. Five experts in thoracic radiology in these extramural reviews diagnosed ILD in 64 patients. Multivariate analysis indicated that the predictive risk factors for the development of ILD were as follows: male, smoking and existence of idiopathic pulmonary fibrosis. However, this group did not review CT films of the chest in all 1976 patients. How much interstitial shadow on chest CT impacts ILD development remains unknown.

ILD has a high associated risk of death, even if steroid therapy resolves ILD temporarily. Furthermore, ILD affects salvage chemotherapy. In cases where patients are at a high risk of developing ILD, anti-cancer drugs that tend to cause ILD should be avoided. Previous analysis often included only those cases developing ILD, but not all cases undergoing chemotherapy (4,5). The frequency of interstitial shadow in

For reprints and all correspondence: Seiji Niho, the Division of Thoracic Oncology, National Cancer Center Hospital East, Kashiwanoha 6-5-1, Kashiwa, Chiba 277-8577, Japan. E-mail: siniho@east.ncc.go.jp

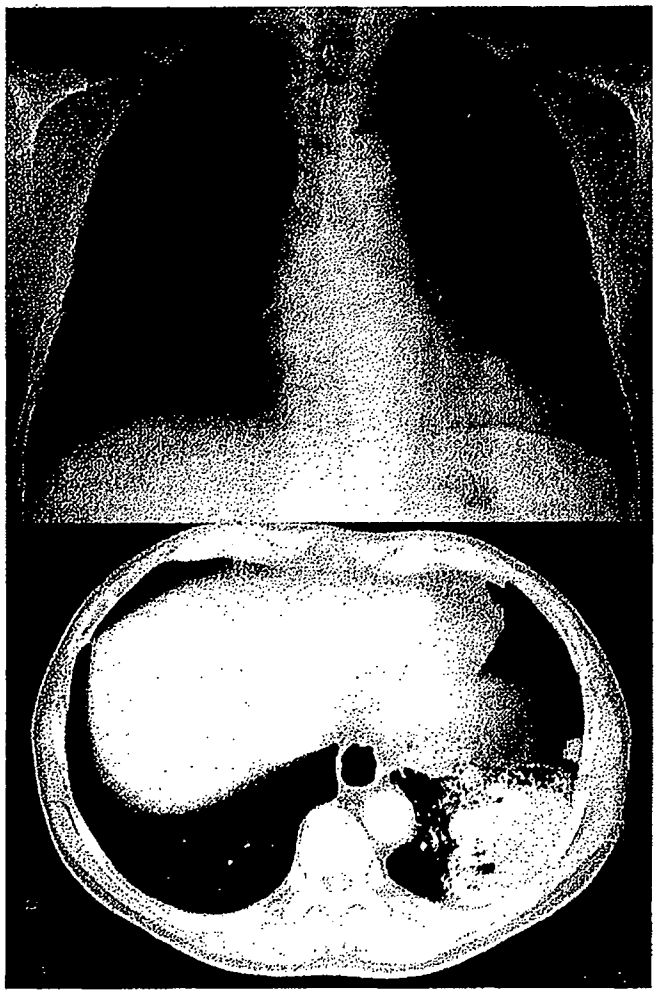

Figure 1. Mild interstitial shadow. An X-ray film of the chest shows no obvious interstitial shadow. A CT film of the chest demonstrated ground-glass opacity in the right basal lung. Interstitial shadow is classified as mild in this case.

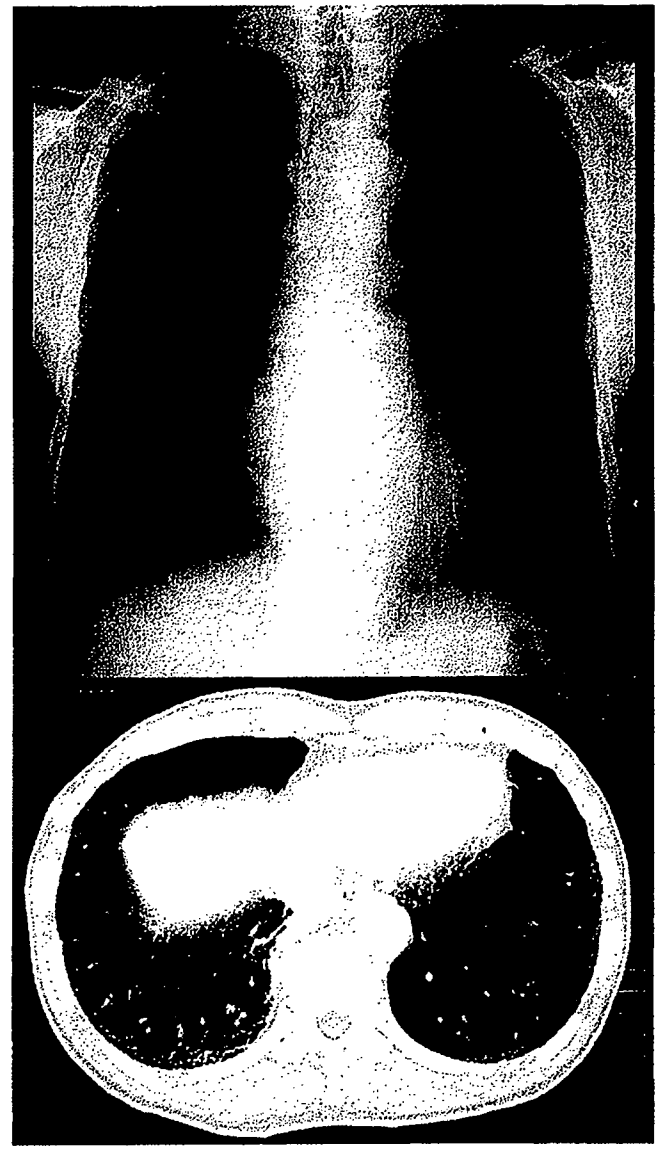

Figure 2. Moderate interstitial shadow. An X-ray film of the chest shows bilateral reticular shadow in the basal area. A CT film of the chest demonstrated bilateral reticular shadow just below the pleura. Interstitial shadow is distributed in 10–30% of the bilateral lower lobes, with this being classified as moderate.

pretreatment CT films of the chest in patients with lung cancer remains unknown, and also how much interstitial shadow confers a risk toward ILD. To further clarify the influence of interstitial shadow on developing ILD, we retrospectively analyzed pretreatment CT films of the chest in consecutive lung cancer patients receiving chemotherapy.

PATIENTS AND METHODS

We retrospectively reviewed the medical records of lung cancer patients who began to receive first-line chemotherapy between October 2001 and March 2004 at the Division of Thoracic Oncology in the National Cancer Center Hospital East. Patients who received thoracic radiotherapy to the primary lesion, mediastinum, spinal or rib metastases were excluded. Plural pulmonologists (S.N., Y.H.K., K.Y., and K.G.) reviewed pretreatment conventional CT and plain X-ray films of the chest. Whether patients had developed ILD or not was blinded to the pulmonologists when they read the films. Conventional spiral CT films were used in our analysis, as high-resolution CT was not routinely conducted. Ground-glass opacity, consolidation or reticular shadow without segmental distribution was defined as interstitial shadow. Localized low attenuation area was defined as emphysema. The grading criteria for interstitial shadow was mild (<10% in bilateral lower lobes), moderate (10–30% in bilateral lower lobes) and severe (>30% in bilateral lower lobes) (Figs 1, 2, and 3). These breakpoints (10 and 30%) were chosen for convenience sake. Interstitial shadow detected on CT films of the chest, but not on plain X-ray, corresponded to mild interstitial shadow. The grading criteria for pulmonary emphysema were mild (<10% in bilateral lungs), moderate (10–30% in bilateral lungs) and severe (>30% in bilateral lungs).

Figure 3. Severe interstitial shadow. An X-ray film of the chest shows bilateral reticular shadow. Reticular shadow is distributed in >30% of the bilateral lower lobes, with this being classified severe.

We identified patients developing ILD, utilizing medical records. ILD was diagnosed on the basis of standard or high-resolution CT findings of the chest (diffuse ground-glass opacity, reticular shadow or consolidation without segmental distribution), elevation of serum levels of lactate dehydrogenase (LDH) and/or KL-6, and lack of response to antibiotics. Bronchoalveolar lavage had not been performed to rule out infections. Most patients diagnosed as ILD were treated with corticosteroids. We compared patients who either had or had not developed ILD in terms of existence and severity of interstitial shadow, emphysema and/or pulmonary bullae on CT films of the chest, as well as patient characteristics including age, gender, smoking history and regimens of received chemotherapy. Comparisons between proportions were performed using a Fisher exact test or a Pearson chi-square test, as appropriate. Multivariate analyses were performed using the logistic regression procedure to determine the relationship between several factors and the onset of ILD.

RESULTS

A total of 502 patients were eligible, with the relevant patient characteristics shown in Table 1. A total of 74% of patients were male and 84% of patients had NSCLC, while the remaining 16% had small cell lung cancer; 79% of the patients were smokers, while 21% never smoked. Platinum-based chemotherapy was performed on 384 patients (76%). A total of 188 patients (37%) received tyrosine kinase inhibitor (TKI) treatment, namely gefitinib or erlotinib. TKI therapy was administered as a first-line (n = 48), second-line (n = 68), third-line (n = 62), fourth-line (n = 9) or fifth-line (n = 1) regimen. Out of 48 patients treated with TKI as a first-line treatment 41 had been entered into a phase II trial of single agent treatment with gefitinib (6).

Radiological findings on this patient cohort are listed in Table 2. Interstitial shadow was detected on chest X-ray and CT in 13 and 20% of patients, respectively. Mild, moderate or severe interstitial shadow was identified in 7, 8 or 5% of patients. Pulmonary emphysema was detected in 38% of patients. Mild, moderate or severe pulmonary emphysema was detected in 18, 10 or 10% of patients. Pulmonary bullae were detected in 20% of patients.

Twenty-six patients (5.2%) developed ILD either during or after chemotherapy. The last regimen of chemotherapy received prior to the onset of ILD included platinum plus vinorelbine or gemcitabine (n = 4), platinum plus taxane (n = 4), other platinum-based chemotherapy (n = 2), vinorelbine plus gemcitabine (n = 2), docetaxel plus gemcitabine (n = 2), single agent treatment with taxane (n = 2) and TKI treatment (n = 10). Out of 26 patients who developed ILD, 14 had a history of taking TKI. Four patients developed ILD after first- or second-line chemotherapy with TKI followed by combination chemotherapy of cisplatin plus vinorelbine (n = 2) or single agent treatment with docetaxel (n = 2).

Univariate analyses demonstrated that male gender (P = 0.0361) and interstitial shadow on CT films of the chest (P = 0.0096) were significantly associated with the onset of ILD (Tables 1 and 3). Multivariate analyses showed interstitial shadow on CT films of the chest [odds ratio (OR): 3.20, 95% confidence interval (CI): 1.34–7.59] and treatment history with gefitinib or erlotinib (OR: 3.17, 95% CI: 1.36–7.36) were associated with the onset of ILD. Male gender was not a significant risk factor for development of ILD in multivariate analysis (OR: 4.33, 95% CI: 0.97–19.38) (Table 4). Univariate and multivariate analyses demonstrated that neither interstitial shadow on X-ray films nor the number of chemotherapy regimens was associated with the onset of ILD.

DISCUSSION

Pulmonary fibrosis or interstitial pneumonia is considered to be a risk factor for ILD caused by drugs (5). In line with the